CORROSION SCIENCE AND TECHNOLOGY, Vol.18, No.2(2019), pp.39~48
[Research Paper]
pISSN: 1598-6462 / eISSN: 2288-6524
DOI: https://doi.org/10.14773/cst.2019.18.2.39

Pitting Corrosion Inhibition of Sprinkler Copper Tubes via Forming of Cu-BTA Film on the Inner Surface of Corrosion pits

Sang Hee Suh[1,†], Youngjoon Suh[1], Sohee Kim[2], Jun-Mo Yang[3], and Gyungtae Kim[3]

[1]*Suh and Suh Corrosion Engineering, Daewangpangyo-ro 606-gil 31, Bundang-gu, Gyunggi-do 13524, Republic of Korea*
[2]*Advanced Analysis Center, Korea Institute of Science and Technology, 5 Hwarang-ro 14-gil, Seongbuk-gu, Seoul 02792, Republic of Korea*
[3]*National Nanofab Center of Korea, 291 Daehak-ro, Yuseong-gu 34141, Republic of Korea*

(Received February 20, 2019; Revised April 06, 2019; Accepted April 09, 2019)

The feasibility of using benzotriazole (BTAH) to inhibit pitting corrosion in the sprinkler copper tubes was investigated by filling the tubes with BTAH-water solution in 829 households at an eight-year-old apartment complex. The water leakage rate was reduced by approximately 90% following BTAH treatment during 161 days from the previous year. The leakage of one of the two sprinkler copper tubes was investigated with optical microscopy, scanning electron microscopy, energy dispersive spectroscopy, X-ray photoelectron spectroscopy, and X-ray diffraction analysis to determine the formation of Cu-BTA film inside the corrosion pits. All the inner components of the corrosion pits were coated with Cu-BTA films suggesting that BTAH molecules penetrated the corrosion products. The Cu-BTA film was about 2 nm in thickness at the bottom of a corrosion pit. A layer of CuCl and Cu_2O phases lies under the Cu-BTA film. This complex structure effectively prevented the propagation of corrosion pits in the sprinkler copper tubes and reduced the water leakage.

Keywords: *Copper, Pitting corrosion inhibition, Benzotriazole, EDS, XPS*

1. Introduction

Many wet sprinkler systems installed with copper tubing in Korea have been suffering from water leakage for the last 10 years due to pitting corrosion failure of copper tubes [1,2]. Pressurized air remaining over water in the copper tubing of the wet sprinkler systems have made the copper tubes vulnerable to pitting corrosion [1], just like stagnant water with an air pocket causes water line corrosion in the water supply system [3]. Sediment deposition at the bottom of copper tubes was identified as another cause of pitting corrosion failure of the sprinkler copper tubes [2,4].

There are inorganic and organic corrosion inhibitors used for copper. Chromates, molybdates and tetraborates belong to the inorganic corrosion inhibitors for copper. Inorganic inhibitors have an advantage over organic inhibitors in that they are stable over a relatively wide temperature range [5], while they have some shortcomings such as toxicity and weak corrosion inhibition efficiency [6]. Organic corrosion inhibitors are more popular because of their much higher corrosion inhibition efficiency than inorganic counterparts. Azole compounds including benzotriazole (BTAH), amine, and amino acid are the most important organic corrosion inhibitors for copper [6]. BTAH has been known for more than 70 years since 1947 [7] as the most effective corrosion inhibitor for copper and its alloys. When copper or its alloy is immersed in a BTAH solution, a protective layer of polymerized Cu-BTA complex is formed rapidly either on copper oxide or copper surface which prevents corrosion reaction. It has been used not only for industrial applications where copper is almost free of corrosion, but also for conservation of archaeological artifacts suffering from corrosion since Madsen first used BTAH in this field in 1967 [8]. BTAH is classified as a mixed type inhibitor since it suppresses both oxygen reduction and copper oxidation [9,10]. Synergistic effects of a combination of BTAH with other organic compounds have been studied by Golfomitsou and Merkel [11].

Initiation of corrosion pits in freshly installed copper can be prevented by using a corrosion inhibitor generating a high pitting potential such as BTAH [12]. However, it is believed that once corrosion pits are initiated on the copper tube, it is difficult to stop their propagation up to the stage of pin hole formation and water leakage. It

† Corresponding author: suhandsuh@outlook.kr

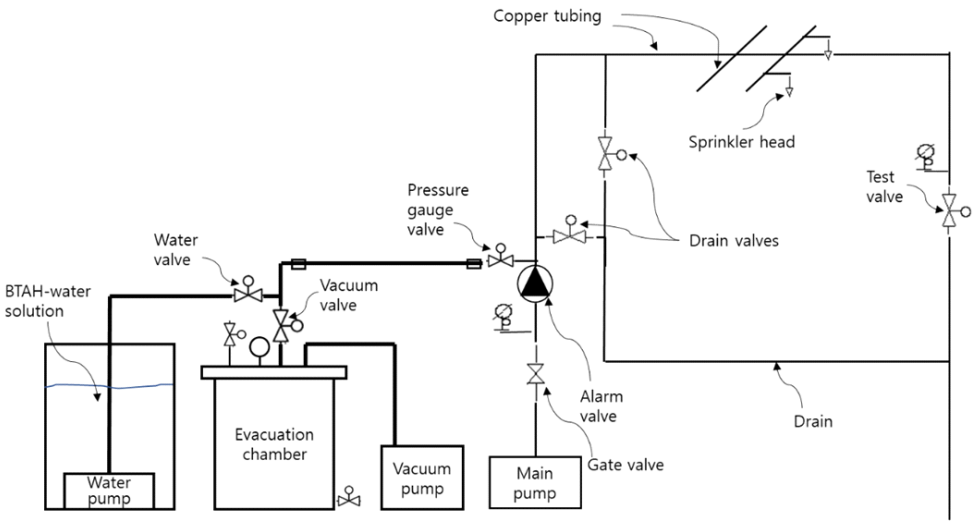

Fig. 1 Schematic diagram of the system for filling BTAH-water solution in the sprinkler copper tubing after vacuum evacuation.

is not clear whether BTAH could be effective even for preventing propagation of already existing corrosion pits. The fact that BTAH has been used successfully for the conservation of archaeological objects suffering not just from general corrosion but also from pitting corrosion gives us a hint that BTAH can be used even for preventing propagation of corrosion pits formed in the sprinkler copper tubes. Corrosion pits of copper are covered with a thick cap of different corrosion products of cuprite (CuO), cuprous oxide (Cu_2O), and malachite ($Cu_2(OH)_2CO_3$) particles, which may make penetration of BTAH molecules into the corrosion pits difficult. It is also not sure whether BTAH can form corrosion inhibitive Cu-BTA composite layer on copper or copper oxide inside the corrosion pit which is under a highly acidic as well as chloride ion-containing environment. Musiani and Mengoli [13] showed by an electrochemical and SERS (surface enhanced Raman spectroscopy) that at low pH, BTAH molecules are adsorbed weakly on a copper surface and displaced from surface sites by chloride ions. Brusic *et al.* [14] reported that in acidic BTAH solutions (pH<2) a thick film is formed, which is not protective enough because of poor polymerization of the film. All the research works on the pH dependence of corrosion inhibition of BTAH has been done on clean copper or copper alloys in acidic solutions. However, there has been no such study yet on the formation of corrosion inhibitive Cu-BTA composites inside the corrosion pits, particularly those in the sprinkler copper tubes.

In this study, the authors tried to reduce the occurrence of water leakage in the sprinkler copper tubes by stopping the propagation of corrosion pits, using BTAH. The authors also investigated whether Cu-BTA film was formed well on the inner structure of the corrosion pits of one sprinkler copper tube by using optical microscopy, scanning electron microscopy (SEM), energy dispersive spectroscopy (EDS), X-ray photoelectron spectroscopy (XPS), and X-ray diffractometry (XRD).

2. Experimental procedures

2.1 BTAH treatment of copper tubes in the wet sprinkler system

Copper tubes of 277 wet sprinkler systems for the total of 829 households at an 8-year old apartment complex were filled with 400 ppm BTAH-water solution after vacuum evacuation of the tubes from the pressure gauge valve on the sprinkler alarm valve, using a patent technique [15] and a system shown in Fig. 1. The copper tubes could be filled with BTAH-water solution without air pockets forming in the copper tubes. Some sediments at the bottom of the tubes could be removed as well by vacuum evacuation. The purity of BTAH (CAS No. 95-14-7) was better than 99.0%, as specified by the manufacturer, Samchun Chemicals of Korea. Water leakage from the sprinkler systems of the households was monitored for 161 days.

A piece of the copper tubing was cut from the apartment fire sprinkler system which leaked water after being filled with 400 ppm BTAH-water solution for 36 days. Small specimens with corrosion pits were cut from the copper tube by a saw and used for microscopical, compositional

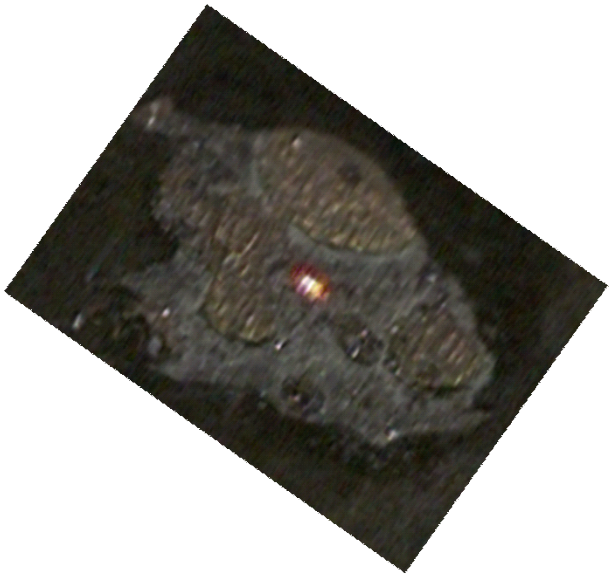

Fig. 2 Alignment of the specimen for the micro-XRD measurement with the help of a laser beam; the bright spot at the center shows the laser beam on the corrosion pit found in the region 3 (see Fig. 5).

and structural characterization of the corrosion pits.

2.2 Microscopical, compositional and structural characterization

The general morphology of the corrosion pits was examined by optical microscopy. SEM and EDS of a FEI Inspect F50 system and a Hitachi Regulus 8230 were used to characterize the surface morphology and measure the composition of the inside of the corrosion pits in the copper tube. The acceleration voltage of 10 kV was used for the SEM and EDS analyses. XPS of a ThermoFisher Scientific K-Alpha+ was used to measure the surface composition and depth profile of the inside of corrosion pits after the cap of corrosion products was removed. The size of the X-ray source for the XPS analysis was 200 μm in diameter. Ar ion sputtering with an Ar ion gun energy of 500 eV and 10 mA was used for depth profile. The sputtering rate for the depth profile that was based on the SiO_2 sputtering rate was 1.25 nm s^{-1}. A micro-XRD of D8-discover was used to identify the materials in the corrosion pits using Cu Kα radiation at 40 kV and 40 mA. A rough estimate by Beer-Lambert law for attenuation of X-ray gives the XRD analysis depth of 60 μm. The X-ray beam size on the specimen was 800 μm in diameter. The exact position of the micro-XRD measurement was selected by moving the X-Y stage with the help of a laser beam as shown in Fig. 2.

3. Results

3.1 Decrease of water leakage rate of the wet sprinkler systems by the BTAH treatment

Each of the sprinkler systems for the 829 households has been filled with 400 ppm BTAH-water solution for 142 days on the average. During the monitoring of 161 days, water leakage occurred from only two households, 36 and 133 days, respectively, after filled with BTAH-water solution in their sprinkler systems. This is about 90% reduction from a year earlier in the water leakage rate at this apartment complex.

3.2 Characterization of corrosion pits on a sprinkler copper tube treated with BTAH

The sprinkler copper tube in the ceiling of a living room which leaked water 36 days after it was filled with BTAH-water solution was cut and studied. Fig. 3 shows the outer surface of the sprinkler copper tube of 25 mm in inner diameter from which water leaked. The tube was

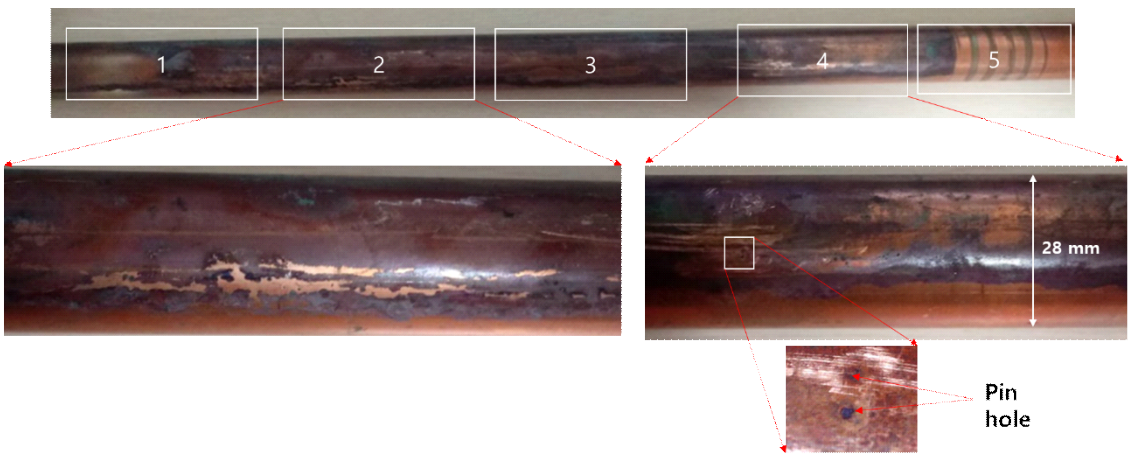

Fig. 3 The outer surface of the sprinkler copper tube which leaked after being filled with BTAH-water solution for 36 days.

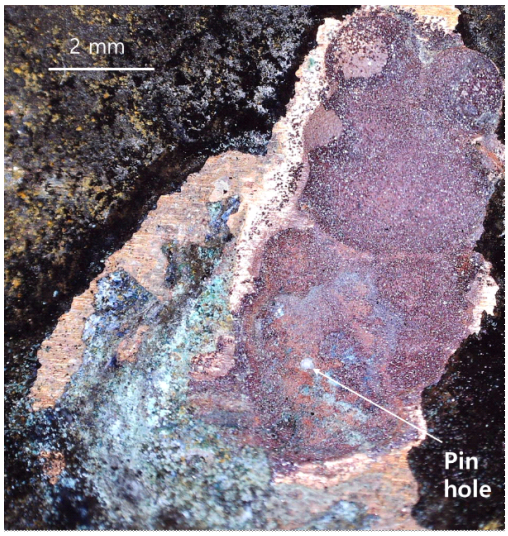

Fig. 4 The inner structure of the corrosion pits from which water leaked.

divided into four regions for identification.

The two pin holes through which water leaked are shown on the outer surface in region 4 of Fig. 3. Fig. 4 shows the inside morphology of the corrosion pit containing two pin holes. All the corrosion products were removed by a tweezer for visual inspection. As small corrosion pits grew, they were probably combined to become two giant corrosion pits. The inside surface of the corrosion pits is covered with dark red cuprous (Cu_2O) particles. It seems that as the giant corrosion pit at the bottom became so wide and deep (about 4 mm in width and more than 1 mm in depth), the thickness of the tube became very thin, forming pin holes. The bigger pin hole is shown as a white dot in Fig. 4.

The corrosion pits found in regions 2 and 3 were studied thoroughly by optical microscopy, SEM, EDS, XPS, and XRD. Fig. 5a is the optical microscopic image of the corrosion pit in region 3 before removing its cap. Fig. 5b and c are the optical microscopic and SEM images, respectively, taken after the cap of the corrosion pit was removed. Table 1 shows the composition measured by EDS of areas A~D indicated in Fig. 5b and c. At area A which is the rim part of the cap consisting of bluish

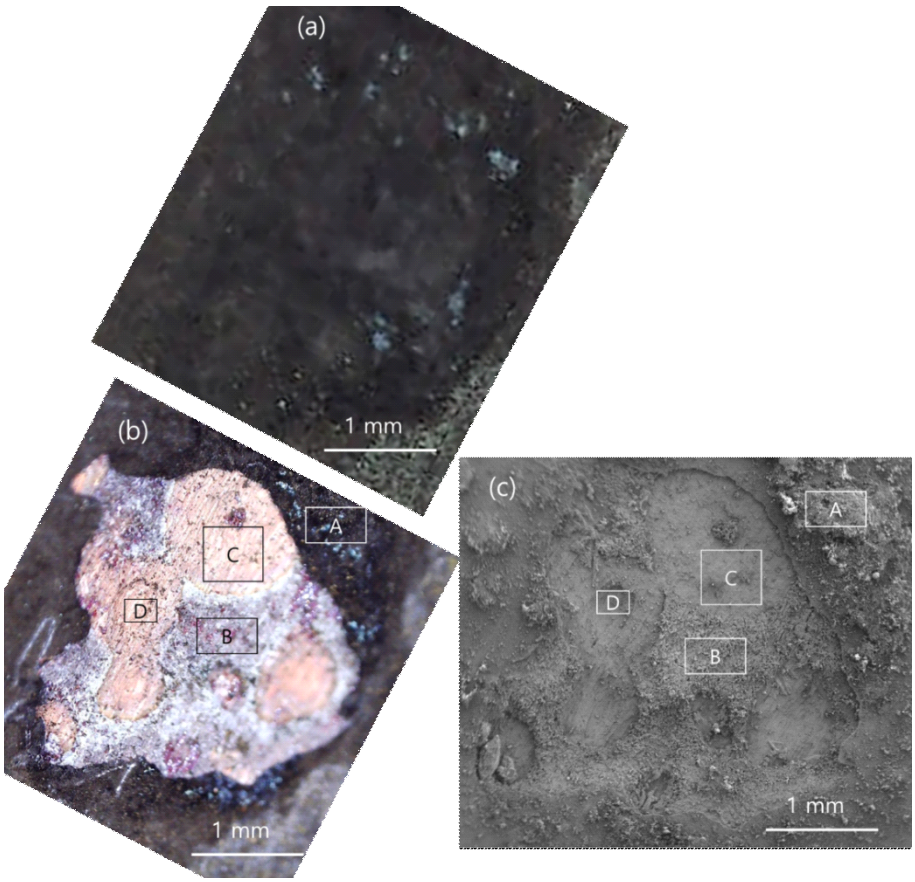

Fig. 5 Corrosion pit found in region 3: (a) optical microscopic picture before the cap was removed; (b) optical microscope and (c) SEM pictures after the cap was removed.

Table 1 EDS analysis results of A~D areas marked in Fig. 5 (at.%)

Element \ Position	A	B	C	D
C	33.0	11.9	4.7	7.2
N	9.9	1.3	-	0.5
O	31.7	25.9	12.8	12.2
Cu	25.4	34.4	82.5	80.1
Cl	-	26.6	-	-

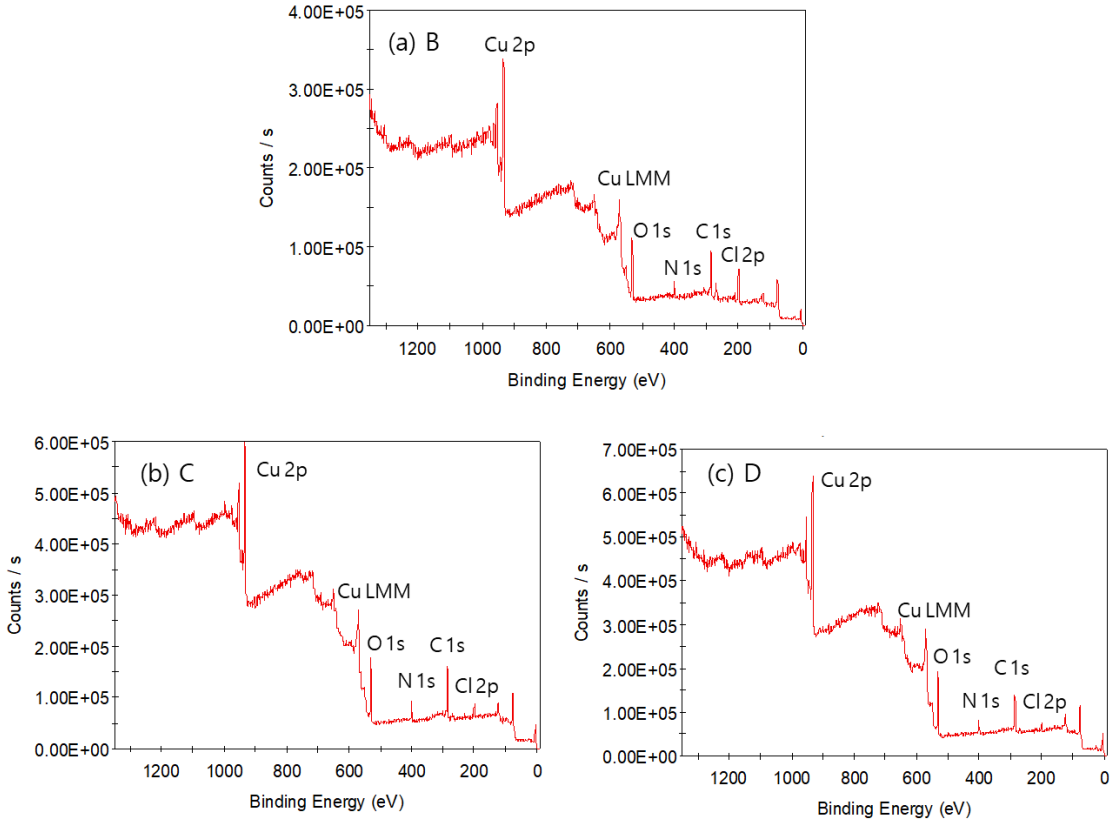

Fig. 6 XPS survey spectra at areas (a) B, (b) C, and (c) D indicated in Fig. 5.

green malachite ($Cu_2(OH)_2CO_3$) particles and black cuprite (CuO) particles, a high nitrogen concentration near 10 at.% is measured. At area B under the malachite layer, the nitrogen concentration was 1.3 at.%. Area B has a very high concentration of chlorine. It is generally believed that chloride ions are attracted into the corrosion pit by the positive ions of hydrogen and copper generated in the pit during the propagation stage [16]. No nitrogen was measured by EDS at area C which looks like the copper base material just under the Cu_2O layer, while a small concentration of nitrogen was measured at the small pit D. Chlorine was not detected by EDS at areas C and D.

Because the EDS analysis depth with the acceleration voltage of 10 KeV is around 1 μm, the EDS analysis results in Table 1 are only the average concentrations over the volume as big as 1 μm in depth. In order to study the surface structure of areas B, C and D, XPS survey spectra of those areas were obtained as presented in Fig. 6. XPS peaks observed are Cu 2p, Cu LMM, O 1s, N 1s, C 1s, and Cl 2p. The appearance of the N 1s peak as well as the high C 1s peak in the XPS spectra indicates that the Cu-BTA film was formed on the surface. The C 1s spectrum for area C (Fig. 7) shows two peaks, one at 284.5 eV with high intensity and the other around 288.5

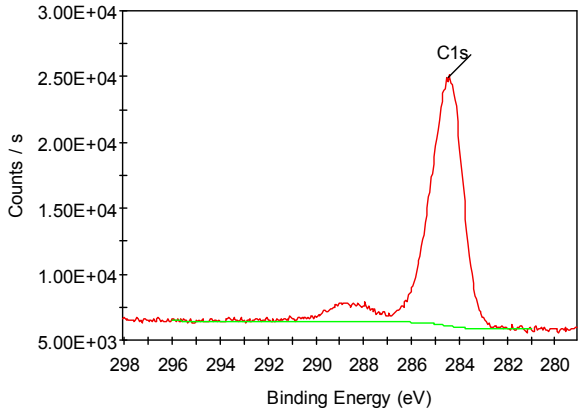

Fig. 7 C 1s XPS spectrum at area C.

Table 2 Surface concentrations at areas B, C, and D measured by XPS (at.%)

Position / Element	B	C	D
C 1s	38.7	45.5	41.8
N 1s	9.6	9.6	8.7
O 1s	22.2	22.6	26.4
Cu 2p	19.1	18.3	20.2
Cl 2p	10.4	4.0	3.0

eV. The intense C 1s peak at 284.5 eV is due to carbon in the aromatic ring of BTAH molecule [17,18] while the broad peak around 288.5 eV may be from contaminant carbon [19]. The surface concentrations at these areas obtained by XPS are given in Table 2. The chlorine composition at area B is higher than those at areas C and D. At areas C and D, about 20 at.% copper, about 9 at.% nitrogen and more than 40 at.% carbon was measured by XPS while about 80 at.% copper, almost no nitrogen, and less than 8 at.% carbon was measured by EDS. These differences between the XPS and EDS results indicate that a very thin Cu-BTA film consisting of carbon, nitrogen, and copper was formed at the surface. The XPS analysis depth is as large as 10 nm [20]. Therefore, detection of oxygen, copper, and chlorine at the surface by XPS may not mean that copper oxide and chloride compounds are embedded in the thin Cu-BTA film whose thickness is less than 5 nm, as shown later in the XPS depth profiles of area B in region 3 and area I in region 2 (Fig. 8 and Fig. 12). The position of these compounds in the whole structure will be discussed in the next paragraph.

Fig. 8 shows the XPS depth profile of area B. Since the etch depth in the XPS depth profile was converted from the sputtering time based on the sputtering rate of

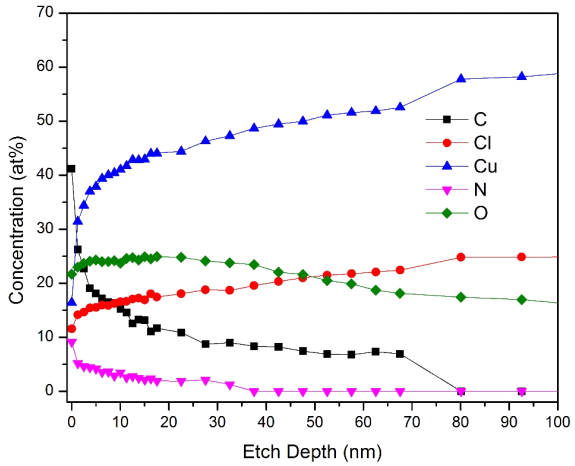

Fig. 8 XPS depth profile of area B of the corrosion pit found in region 3.

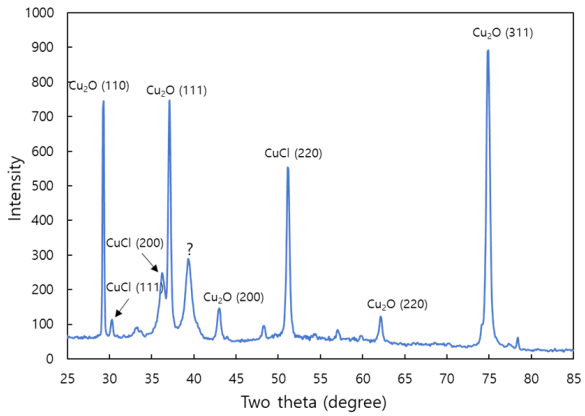

Fig. 9 XRD spectrum of area B of the corrosion pit found in region 3.

SiO_2, there could be some discrepancy between the etch depth and the converted one. The nitrogen concentration is about 10 at.% at the surface. It decreases continuously to 0 at.% up to 37 nm, and it is not detected at the larger depth. The Cu-BTA film thickness may be much smaller than 37 nm, however, because the unevenness of area B could have made nitrogen detected even at the etch depth larger than the Cu-BTA film thickness. Instead, the etch depth at the inflection point of the composition profile of nitrogen which is 2 nm could be considered as the thickness of the Cu-BTA film. The high oxygen concentration measured at the outermost layer of the surface may mean that oxygen atoms of the underlying Cu_2O layer are located almost at the same depth as the constituent elements of the Cu-BTA film as a model of the Cu-BTA film on Cu_2O shows [21]. The chlorine concentration increases rapidly in the surface region of 5 nm in depth. Considering that the XPS analysis depth is as large as

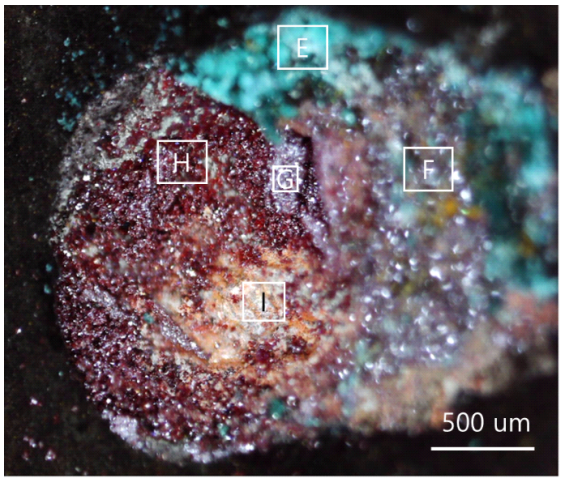

Fig. 10 Optical microscope image of the corrosion pit found in region 2 after the left half of the cap was removed.

10 nm, this rapid increase of the chlorine concentration at the surface may mean that the chloride compound is not included in the Cu-BTA film. In other words, the chlorine concentration measured at the zero etch depth might have come from the layer underneath the Cu-BTA film, not from the outermost Cu-BTA film. A high chlorine concentration more than 25 at.% was measured at the etch depth larger than 80 nm, which is consistent with the EDS result of Table 1. At the etch depth larger than 130 nm (not shown in Fig. 8), the ratio of chlorine to oxygen concentrations is close to 2.

Since a high chlorine concentration more than 25 at.% was measured by both EDS and the XPS depth profile, it would be interesting to study the structure of the chloride compound under the Cu-BTA film. An X-ray diffraction pattern of Cu_2O and CuCl peaks was obtained on the surface of area B (Fig. 9). This result is consistent with the XPS depth profile in which only copper, chlorine, and oxygen exist at the etch depth larger than 80 nm. The strong peaks of Cu_2O and weaker peaks of CuCl indicate that the Cu_2O layer is beneath a composite of CuCl and Cu_2O. The peak marked with '?' could not be identified.

It was confirmed by the XPS measurements on areas B, C, and D in region 3 that all parts of the corrosion pit in region 3 are coated well with Cu-BTA films. This was only possible because BTAH molecules could penetrate the corrosion pit through all corrosion products including CuO, $Cu_2(OH)_2CO_3$, and Cu_2O layers.

To confirm whether the deep position of the corrosion pit found in region 2 was coated with the Cu-BTA film, the corrosion products in the left half of the corrosion pit shown in Fig. 10 were scraped off by a tweezer. The areas indicated by the symbols of E, F, G, H, and I in Fig. 10 were analyzed by EDS (Table 3). The depths of these positions are in the alphabetical order. In other words, area E is at the shallowest location in the corrosion pit while area I is at the deepest location in the corrosion pit. Nitrogen was detected on all positions analyzed. The deeper the position in the corrosion pit is, the smaller the nitrogen composition becomes. Areas E and F consisting of bluish green malachite particles and dark red cuprous oxide particles have relatively high nitrogen concentration. Noticeable chlorine concentrations of 4.1 and 23.3 at.% were detected at areas H and I, respectively. The H is the area where Cu_2O particles are gathered together while the I is the bottom of the corrosion pit from which almost all Cu_2O particles were scraped off.

To confirm whether the Cu-BTA film was formed at the two deepest positions, H and I, XPS survey spectra and surface concentrations of these areas were obtained as presented in Fig. 11 and Table 4, respectively. The small N 1s peaks (about 5 at.%), as well as the high C 1s peaks (more than 40 at.%), show that the Cu-BTA film was formed well on the surface of these two deep regions. Fig. 12 shows the XPS depth profile of area I. The nitro-

Table 3 EDS analysis results of the areas E~I marked in Fig. 7 of the corrosion pit found in the region 2 (at.%)

Element \ Position	E	F	G	H	I
C	21.1	19.9	1.8	15.9	18.0
N	1.3	2.2	0.8	0.8	0.5
O	55.1	43.3	29.8	32.0	8.4
Cu	21.4	34.4	67.6	47.1	49.8
Cl	-	0.3	-	4.1	23.3
S	1.1	-	-	-	-

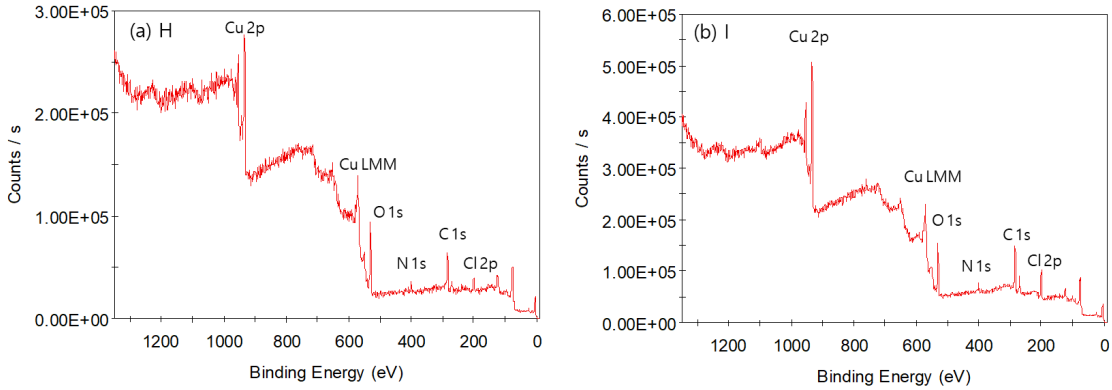

Fig. 11 XPS survey spectra at areas (a) H and (b) I.

gen concentration is 5 at.% at the surface, and it is not detected at the etch depth larger than 2 nm, indicating that a Cu-BTA film thinner than 2 nm was formed on the surface. The carbon and oxygen concentrations also decrease rapidly while the copper and chlorine concentrations increase rapidly on the outermost layer of the surface. Detection of oxygen and chlorine at the surface does not necessarily mean that oxygen and chloride compounds are embedded in the Cu-BTA film for the same reason given when interpreting the XPS depth profile of area B of the corrosion pit in region 3. At the etch depth larger than 5 nm, the ratio of chlorine to oxygen concentrations is close to 2, just like at area B of the corrosion pit in region 3.

Table 4 Surface atomic concentrations at areas H and I measured by XPS (at.%)

Element \ Position	H	I
C 1s	40.9	44.3
N 1s	5.4	5.0
O 1s	28.9	22.3
Cu 2p	19.0	19.0
Cl 2p	5.8	9.4

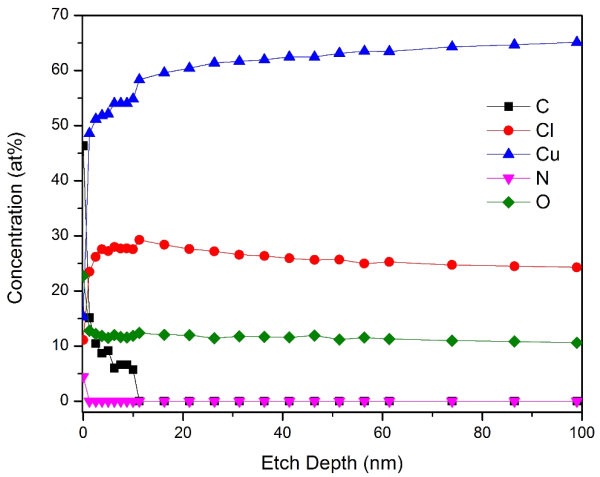

Fig. 12 XPS depth profile of area I of the corrosion pit found in region 2.

The area I was analyzed by micro-XRD, and Fig. 13 shows its XRD spectrum. Peaks of comparable heights were observed for Cu and Cu_2O, indicating that a thin Cu_2O layer is present on the Cu base material. It should be noticed that CuCl peaks were also observed, which is consistent with the detection of more than 23 at.% Cl by both EDS analysis and the XPD depth profile. The peak marked as '?' in Fig. 13 could not be identified.

3. Discussion

Based on the information gathered by EDS, XPS, and XRD analyses, we propose the schematic structure of Fig. 14 for the Cu-BTA film and the underlying materials formed inside the corrosion pit of the sprinkler copper tube. The outermost layer is the Cu-BTA film with the underlying layer of Cu_2O and CuCl phases sitting on the Cu_2O layer. If the chloride concentration in the water inside the corrosion pit is diluted, the layer of Cu_2O + CuCl in the structure will shrink in thickness, which is the case for areas C and D of the corrosion pit in region 3. The way how this kind of structure could be formed in the chloride containing water by BTAH is discussed in the next paragraph.

In metallic materials such as Fe and Cu, chloride ions are attracted electrically into the corrosion pits by positive metallic ions and hydrogen ions, accelerating the growth of corrosion pits [16,22]. Several research groups dis-

cussed the mechanism of how chloride ions suppress rather than accelerate corrosion of copper in the presence of BTAH. BTAH has been known for a long time to behave as an efficient corrosion inhibitor of copper in chloride solutions [23,24]. Evans *et al.* [25] explained the corrosion inhibition effect of BTAH in chloride solutions by formation of a CuCl layer on the surface of Cu which interacts with BTAH molecules. This blocking substance would render high efficiency of corrosion inhibition. Hashemi *et al.* [26] examined the surface layer formed on copper immersed in a 3 wt% NaCl solution containing BTAH by using XPS and X-AES (X-ray induced Auger spectroscopy). They concluded that a CuCl layer is formed on Cu and this CuCl layer acts as a base layer for formation of the Cu-BTA composite layer whose thickness is determined during the stage of CuCl formation.

On the other hand, Tromans *et al.* [27] showed that a Cu-BTA composite layer could be grown on Cu in the presence of $CuCl_2^-$. According to their mechanism, a monolayer of Cu-BTA is formed on the copper surface. Then, $(Cu\text{-}BTA)_n$ composite is formed by the help of $CuCl_2^-$ within the diffusion distance of $CuCl_2^-$. Finally, this composite is joined to the Cu-BTA monolayer forming the final Cu-BTA composite layer.

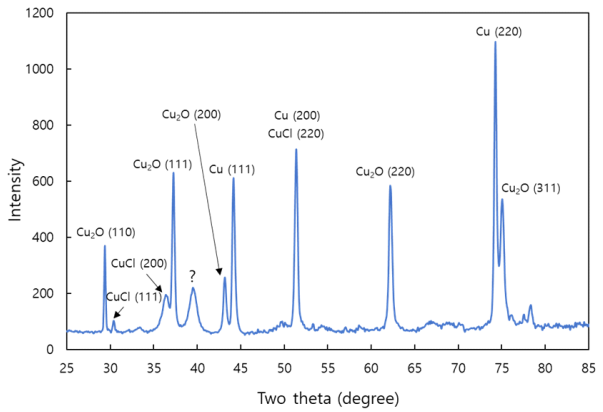

Fig. 13 XRD spectrum of area I of the corrosion pit found in region 2.

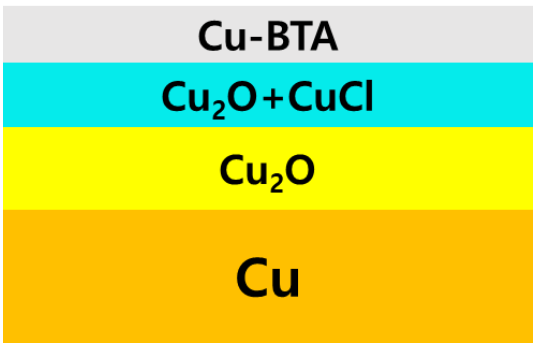

Fig. 14 Schematic structure of the Cu-BTA film and the underlying materials formed inside the corrosion pit of the sprinkler copper tube.

According to the above three mechanisms chloride should be present in the solution for formation of the Cu-BTA protective layer on pure Cu without the Cu_2O on the surface. Because Cu_2O particles or layers are always found inside the corrosion pits in the sprinkler copper tubes, there would be no problem in forming the Cu-BTA protective layer inside the corrosion pits. Chloride ions in the solution would make the formation of the Cu-BTA protective layer on the Cu_2O phase inside the corrosion pit a lot easier. Even further, chloride ions became a constituent of the whole structure by forming the CuCl phase. What is implied in the schematic structure of Fig. 14 is that Cu needed to form the CuCl phase is supplied from the Cu_2O layer on the Cu material rather than from Cu^+ in the water. In other words, some parts of the Cu_2O layer are replaced with CuCl by a reaction between the Cu_2O layer and chloride ions in water. The composition profile in Fig. 12 follows this schematic structure given in Fig. 14. Milosev and Kosec [28] and Rao *et al.* [18] also reported that the Cu-BTA protective layer is formed on Cu and Cu-Ni alloy, respectively in the chloride solution. However, they could not observe any CuCl phase in their structure. It seems that the structure of the Cu-BTA complex layer depends delicately on the environment such as chlorine concentration and pH in the solution.

The composite structure of $Cu_2O/(CuCl+Cu_2O)/Cu\text{-}BTA$ formed well inside the corrosion pit of the sprinkler copper tube seems to be useful in preventing corrosion of the copper material in the corrosion pit under the highly acidic and chloride-containing environment.

5. Conclusions

BTAH was successfully used for reducing the water leakage rate of the sprinkler copper tubes at an apartment complex by about 90%. All the inner parts of the corrosion pits of the sprinkler copper tube were coated well with Cu-BTA films, which is believed to have helped to reduce the water leakage rate. The Cu-BTA film is about 2 nm thick at the bottom of the corrosion pit. The Cu-BTA film was formed on a layer consisting of CuCl and Cu_2O phases. This complex structure seems to be useful in stopping the growth of corrosion pits in the sprinkler copper tubes and reducing the water leakage rate resultantly.

Acknowledgements

The authors would like to acknowledge the financial support from Korea Land & Housing Corporation for this research.

References

1. S. H. Suh, Y. Suh, H. G. Yoon, J. H. Oh, Y. Kim, K. Jung, and H. Kwon, *Eng. Fail. Anal.*, **64**, 111 (2016).
2. J-G. Kim, Research report: Study on the cause of copper tube corrosion, The Korean Institute of Surface Engineering (2016).
3. M. Edwards, J. F. Ferguson, and S. Reiber, *J. Am. Water Works Assoc.*, **86**, 74 (1994).
4. S. H. Suh, Y. Suh, and H. Kwon, *Corros. Sci. Tech.*, **16**, 265 (2017).
5. M. M. Antonijevic and M. B. Petrovic, *Int. J. Electrochem. Sci.*, **3**, 1 (2008).
6. A. Fateh, M. Aliofkhazraei, and A. R. Rezvanian, *Arabian J. Chem.*, in press (2017).
7. Procter and Gamble, Ltd., British Patent, **652339** (1947).
8. H. B Madsen, *Stud. in Cons.*, **12**, 163 (1967).
9. I. Dugdale and J. B. Cotton, *Corros. Sci.*, **3**, 69 (1963).
10. C. Fiaud, *Proc. of the 8th European Symposium on Corrosion Inhibitors (8SEIC)*, p. 929, Ferrara, Italy (1995).
11. S. Golfomitsou and J. F. Merkel, *Proc. of Metal 2004*, National Museum of Australia Canberra ACT (2004).
12. E. A. Skrypnikova, S. A. Kaluzhina and L. E. Agafonova, *Int. J. Corros. Scale Inhib.*, **3**, 59 (2014).
13. M. M. Musiani, G. Mengoli, M. Fleischmann, and R. B. Lowry, *J. Electroanal. Chem.*, **217**, 182 (1987).
14. V. Brusic, M. Angelopoulos, and T. Graham, *J. Electrochem. Soc.*, **144**, 436 (1997).
15. Korea Institute of Science and Technology, Apparatus and methods for drain, vent, and water filling for wet type sprinkler systems, Korea Patent, **10-1938819** (2019).
16. D. A. Lytle and M. N. Nadagouda, *Corros. Sci.*, **52**, 1927 (2010).
17. J. F. Moulder, W. F. Stickle, P. E. Sobol, and K. D. Bomben, Handbook of X-ray Photoelectron Spectroscopy, in: J. Chastain, R. C. King Jr. (eds.), Physical Electronics, Inc., Eden Prairie, Minnesota (1995).
18. B. V . Appa Rao, K. Chaitanya Kumara, and Neha Y. Hebalkar, *Thin Solid Films*, **556**, 337 (2014).
19. G. P. Cicileo, B. M. Rosales, F. E. Varela, and J. R. Vilche, *Corros. Sci.*, **41**, 1359 (1999).
20. R Smart, S. McIntyre, M Bancroft, ansd I. Bello, X-ray Photoelectron Spectroscopy, http://mmrc.caltech.edu/SS_XPS/XPS_PPT/XPS_Slides.pdf.
21. A. Kokalj, *Faraday Discuss.*, **180**, 415 (2015).
22. Z. Ahmad, Principles of corrosion engineering and corrosion control, Butterworth-Heinemann, p. 151, Oxford, UK (2006).
23. G. W. Poling, *Corros. Sci.*, **10**, 359 (1970).
24. R. Walker, *Corrosion*, **31**, 97 (1975).
25. U. R. Evans, The Corrosion and Oxidation of Metals, First Supplementary Volume, St. Martin's Press, New York (1968).
26. T. Hashemi and C. A. Hogarth, *Electrochim. Acta*, **33**, 1123 (1988).
27. D. Tromans and R.-H Sun, *J. Electrochem. Soc.*, **138,** 3235 (1991).
28. I. Milosev and T. Kosec, *Chem. Biochem. Eng. Q.*, **23**, 53 (2009).